Experimental and numerical study of heat generation by energy dissipation in a rotating drum filled with particulate material

Rafael L. Rangel[1], Francisco Kisuka[2], Chuan-Yu Wu[2], Catherine O'Sullivan[3], Alessandro Franci[1], Eugenio Oñate[1]

[1] *International Centre for Numerical Methods in Engineering (CIMNE), Polytechnic University of Catalonia*
Barcelona 08034, Spain
rrangel@cimne.upc.edu, falessandro@cimne.upc.edu, onate@cimne.upc.edu
[2] *Dept. of Chemical and Process Engineering, University of Surrey*
Guildford GU2 7XH, United Kingdom
f.kisuka@surrey.ac.uk, c.y.wu@surrey.ac.uk
[3] *Dept. of Civil and Environmental Engineering, Imperial College London*
London SW7 2AZ, United Kingdom
cath.osullivan@imperial.ac.uk

Abstract. This work aims to investigate the generation of heat by dissipation of mechanical energy in particulate flows. The behavior of material in a rotating drum is considered in experimental and numerical analyses. In the physical experiments, the temperature of the particles inside the drum was monitored by means of infrared thermography and the influence of rotation speed and filling ratio was explored. The experimental data were later used to calibrate numerical simulations using the Discrete Element Method (DEM). The numerical results were then analyzed to gain more insights into the mechanisms of heat generation.

Keywords: particulate flow, heat generation, rotating drum, infrared thermography, discrete element method.

1 Introduction

In dynamic granular systems where particles are constantly colliding, sliding and rolling against each other and against boundaries, heat is generated by the dissipation of mechanical energy. This energy dissipation can occur by different mechanisms, such as friction and inelastic collisions. As a consequence, the temperature of the system increases, and this can lead to unexpected side effects. For example, in pneumatic conveying, the formation of thin filaments of melted material (angel's hair) can cause the blockage of filters (Lorenz [1]). In geotechnical engineering, frictional heat can be a major cause of shear failures that results in sudden landslides (Voight and Faust [2]). In this work, heat generation by energy dissipation in particulate flows is explored using a rotating drum, a common industrial application for granular mixes where thermal effects are often relevant (Sun et al. [3]).

In the first part of this study, experimental tests were performed to quantify the temperature rise of steel particles inside the rotating drum. Infrared thermography was used to monitor the temperature of the moving particles; infrared thermography is a non-intrusive method that allows instantaneous scanning of the temperature distribution across a surface. The evolution of these temperature data can be recorded for later analysis. The effects of changing the rotation speed and the filling ratio of the drum were investigated. Temperature increases of up to 5°C were observed after 30 minutes in the small scale experiments conducted in this study. In the second part of this research, the experiments were simulated using the Discrete Element Method (DEM), specifically, the soft-sphere approach proposed by Cundall and Strack [4]. A computer program was developed to perform thermally-coupled DEM simulations. Several numerical models have been implemented to take into account heat transfer by conduction and heat generation by sliding friction, rolling friction and damping forces. Some adjustable parameters required for these models were calibrated according to the experimental results. In this way, aspects of heat generation that are very complex, or even impossible, to measure in the physical experiments could be assessed.

2 Methodology

2.1 Experimental analysis

Figure 1a shows the experimental setup with its main components. A rotating drum is partially filled with particles and set to spin around its (horizontal) longitudinal axis. The inner diameter and thickness of the drum are 250 mm and 12.7 mm, respectively. The flat wall on the back of the drum is made of acrylic and the one on the front surface is a fine metallic mesh with a grid size of 0.42 mm, which is stretched to provide sufficient tension to hold the particles. The annular wall around the circumference of the drum is made of wood and coated with sandpaper on the inner face to increase the friction with the particles. Monodisperse spherical particles with a diameter of 6.35 mm and made of stainless steel were used. The density of the particles is 7750 kg/m^3, the specific heat capacity is 460 J/kg.K, the thermal conductivity is 24.9 W/m.K, the Young's modulus is 200 GPa, and the Poisson's ratio is 0.24.

A thermal camera was placed in front of the drum to monitor the temperature of the particles. Figure 1b shows a snapshot of the thermal image captured at the end of an experiment, where the heated particulate flow is clearly seen. The camera is a FLIR A700-EST model. In order to calibrate the camera and take accurate measurements, the reflected apparent temperature of the setup and the emissivity of the particles were estimated according, respectively, to the *reflector method* and the *reference emissivity material method*, both specified in ISO 18434-1:2008 [5]. Furthermore, the emissivity of the particles was adjusted to take into account the presence of the metallic mesh. The metallic mesh was selected as it is an easily sourced material through which part of the infrared radiation emitted by the particles can pass. Other materials that can transmit infrared radiation, such as silicon and germanium, are either too fragile for this application or only manufactured in small sizes. The values estimated for the raw and adjusted emissivity of the particles are 0.38 and 0.47, respectively.

The effects of the rotation speed and the filling ratio of the drum were explored in this work. Three rotation speeds were considered: 15 rpm, 35 rpm, and 55 rpm. The effect of the filling ratio was studied by using three different numbers of particles: 400, 600, and 800. These quantities of particles roughly correspond to filling ratios of 18%, 27%, and 36%. In order to maximize the reliability of the data, each experimental configuration was repeated five times and the average and standard deviation of these datasets were calculated. The duration of the experiments was set as 30 minutes. Before starting an experiment, the setup was allowed to cool long enough to reach the room temperature, which was controlled and monitored to ensure that its variation had a minimum influence on the results. During the experiments, a thermography software was used to draw a rectangular region of interest (R.O.I.) inside an area of the thermal image that is constantly covered by particles, as seen from Fig. 1b. The mean value of the temperature inside the R.O.I. was recorded every five minutes. This value was taken as the representative temperature of the entire particulate flow, as the temperature distribution is assumed to be uniform over all particles.

(a) (b)
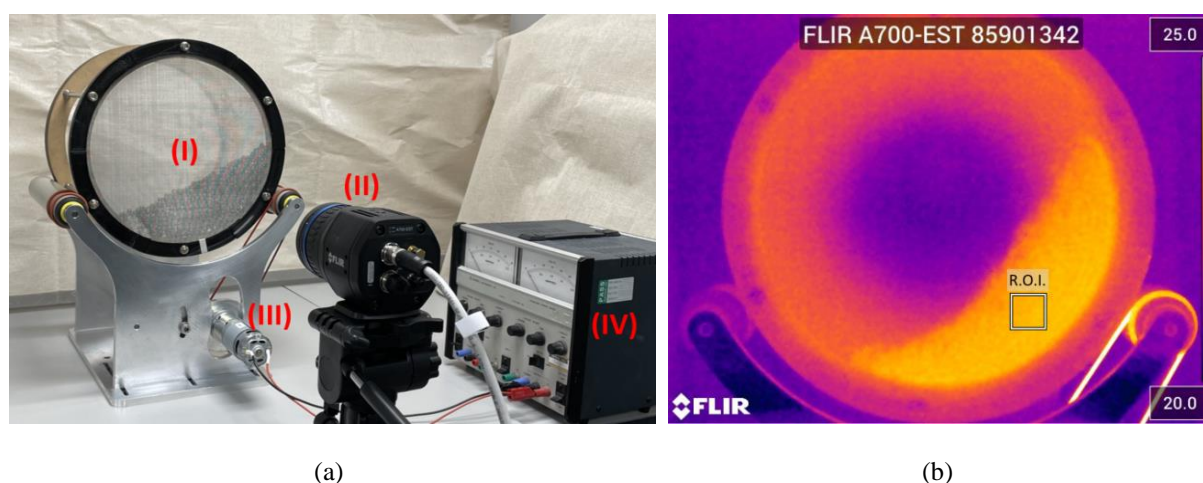
Figure 1. (a) Experimental setup: (I) rotating drum, (II) thermal camera, (III) electric motor, (IV) power supply. (b) Thermal image showing the temperature distribution of the setup at the end of an experiment and the region of interest (R.O.I.) used to measure the temperature of the particulate flow.

2.2 Numerical simulation

A DEM solver for thermomechanical simulations was implemented on the open-source platform *Kratos Multiphysics* (Dadvand et al. [6]). The coupling between both physics was carried out as presented in Rangel et al. [7]. The motion of each particle is solved according to eq. (1) and eq. (2), where m, I, $\vec{v}$, $\vec{\omega}$, $\vec{F}$, and $\vec{M}$ are, respectively, the mass, moment of inertia, translational velocity, rotational velocity, resulting force and torque acting on a particle identified by sub-index i. The thermal behavior of particles is evaluated according to eq. (3), where c_p, T, and Q are, respectively, the specific heat capacity, temperature, and net heat transfer. These equations are solved numerically with an explicit time integration scheme in order to obtain the velocities, displacements, rotations, and temperatures of all particles at each time step

$$m_i \frac{d\vec{v}_i}{dt} = \vec{F}_i \tag{1}$$

$$I_i \frac{d\vec{\omega}_i}{dt} = \vec{M}_i \tag{2}$$

$$m_i c_{p,i} \frac{dT_i}{dt} = Q_i \tag{3}$$

The resulting force acting on a particle is calculated with eq. (4). It originates from the particle weight, where $\vec{g}$ is the gravitational acceleration, and the sum of the contact forces with neighboring elements, which can be particles or walls; these neighbors are identified by sub-index j. The contact force has a normal and a tangential component, with moduli F_n and F_t, acting in the directions defined by the unit vectors $\hat{n}$ and $\hat{t}$ respectively. In each of these directions, the force is composed by an elastic, F^{el}, and a viscous component, F^{vis}, which are simulated by a nonlinear spring-dashpot model following Thornton et al. [8]. The torque acting on each particle is calculated with eq. (5). This toque has a component from the tangential contact forces (calculated using $\vec{R}$, the vector from the particle center to the contact point), and the rolling friction torque, M_r, computed using the directional constant model from Ai et al. [10]. Finally, the net heat transfer for each a particle is calculated with eq. (6). It considers two mechanisms: heat generation by energy dissipation, Q_g, and heat conduction through contact areas, Q_c. Since the generation of heat happens at the contact interface, only a portion of it is absorbed by each element. For identical particles, the heat partition coefficient is taken as 0.5.

$$\vec{F}_i = m_i \vec{g} + \sum_j \left(\left(F_{n,ij}^{el} + F_{n,ij}^{vis} \right) \hat{n} + \left(F_{t,ij}^{el} + F_{t,ij}^{vis} \right) \hat{t} \right) \tag{4}$$

$$\vec{M}_i = \sum_j \left(\vec{F}_{t,ij} \times \vec{R}_{ij} - \vec{M}_{r,ij} \right) \tag{5}$$

$$Q_i = \sum_j \left(0.5 Q_{g,ij} + Q_{c,ij} \right) \tag{6}$$

All dissipative forces and torques contribute to the generation of heat. Therefore, the total heat generation results from the dissipated power due to sliding friction, P_f, rolling friction, P_r, and viscous forces, P_{vis}, as shown in eq. (7). A fraction of the dissipated power is converted into heat, given by a conversion coefficient, λ, which is an adjustable parameter ($0 \leq \lambda \leq 1$). The energy dissipation mechanisms are provided in eq. (8) to eq. (10), where v_n and v_t are the magnitudes of the relative velocity in the normal and tangential directions, and μ_k is the dynamic friction coefficient. Sliding friction dissipation takes place only when the relative motion between elements is in the sliding regime according to Coulomb's law of friction, i.e. $F_t > \mu_s F_n$, where μ_s is the static friction coefficient.

$$Q_{g,ij} = \lambda \left(P_f + P_r + P_{vis} \right) \tag{7}$$

$$P_f = \mu_k F_{n,ij} v_t \tag{8}$$

$$P_r = M_{r,ij} \left| \vec{\omega}_i - \vec{\omega}_j \right| \tag{9}$$

$$P_{vis} = F_{n,ij}^{vis} v_n + F_{t,ij}^{vis} v_t \tag{10}$$

Heat conduction between elements is computed from the model of Batchelor and O'Brien [10], as presented in eq. (11), where k is the thermal conductivity and R_c is the radius of the contact area. To increase the time-step so that the analyses could be completed in a feasible time, the value of the Young's modulus adopted here was lower than the real value by several orders of magnitude. Therefore, the contact radius obtained from the simulations is oversized, which in turn leads to an overestimation of the heat transfer. To overcome this, the contact radius used for estimating the heat conduction, R_c, was related to the contact radius obtained from the simulation, $R_{c,sim}$, through the adjustment factor proposed by Zhou et al. [11] and shown in eq. (12), where $\bar{E}$ is the effective Young's modulus (evaluated with the real and simulation value of the Young's modulus): $1/\bar{E} = (1 - {v_i}^2)/E_i + (1 - {v_j}^2)/E_j$, and v is the Poisson's ratio.

$$Q_c = 4 \frac{k_i k_j}{k_i + k_j} R_c \left(T_j - T_i \right) \tag{11}$$

$$R_c = R_{c,sim} \left(\bar{E}_{sim} / \bar{E}_{real} \right)^{0.2} \tag{12}$$

The Young's modulus used in the simulations presented here was 0.02% of the physical value so that the Young's modulus of the steel particles was set to 40 MPa. All other thermomechanical properties of the particles were the same as in the physical experiments. The walls of the model are discretized into small triangular elements whose properties (Tab. 1) were estimated based on the materials used in the experimental setup, and the same ratio of simulation-to-real value of the Young's modulus was applied. In addition the coefficients of static, dynamic and rolling friction, and restitution had to be calibrated to obtain flow regimes similar to those observed in the experiments; values of 0.8, 0.5, 0.03 and 0.6, were used for both particle-particle and particle-wall interactions.

Initially, in each simulation, the particles were allowed to rest in mechanical equilibrium with the drum stopped, and the temperature of all elements, including walls, was set to 293.15 K. Then simulation of the drum commenced and the temperature of the walls was kept constant throughout the analysis. The only mechanism of heat loss from the system was by conduction between particles and walls. A time-step of 10^{-5} s was employed in all simulations.

Table 1. Thermomechanical properties of wall elements

Property	Acrylic Disk	Metallic Mesh	Wooden Ring
Young's modulus (simulation | real) [MPa]	0.66 | 3300	0.66 | 3300	2.00 | 10000
Poisson's ratio [-]	0.37	0.37	0.30
Thermal conductivity [W/m.K]	0.19	10.00	0.20

3 Results

Figure 2 shows the experimental results. The evolution of the temperature rise of particles, measured with the thermal camera, for different rotation speeds considering the intermediate number of particles (600 particles – a filling ratio of approximately 27%) is given in Fig. 2a. The evolution of temperature for different number of particles, considering the intermediate rotation speed of 35 rpm, is provided in Fig. 2b. The error bars at the measurement times represent the standard deviation of the five datasets obtained for each experiment.

It is clear that an increase in the rotation speed leads to a significant increase in the heat generation and, consequently, in the temperature of the particles. This was expected as the drum rotation speed is directly related to the flow regime of the mixed material, so that changing the speed from 15 rpm to 55 rpm results in a change of the flow regime from rolling to cataracting and, thus, increases both the collision frequency and collision energy (Yang et al. [12]). The drum filling ratio appears to have a less significant influence on the heat generation when compared to the effect of changing the rotation speed. In fact, an increase in the number of particles causes only a slight rise in the flow temperature. This can be explained by the fact that the flow regimes observed in the experiments with different numbers of particles were similar. Therefore, the energy dissipation mechanisms during the interactions are not much affected and the average heat generated per particle does not experience an appreciable variation. It can also be noted that, in all cases, the curves present an asymptotic behavior towards a thermal equilibrium. This is because the system is not thermally insulated, so the rate of heat generation that is absorbed by the particles is balanced with the rate of heat loss to the external environment.

(a)   (b)
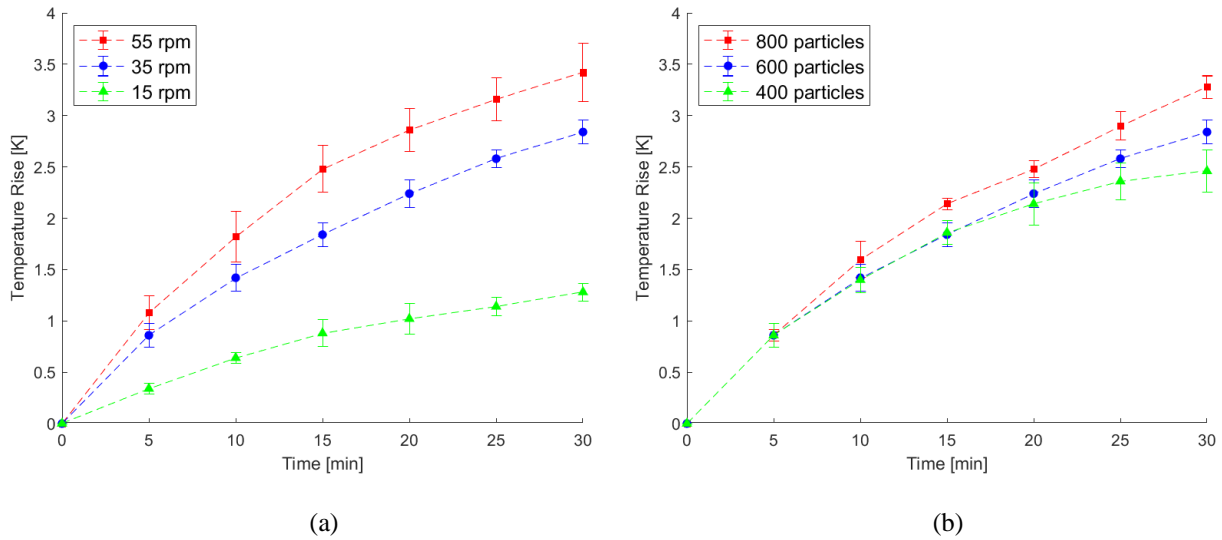
Figure 2. Experimental data giving variation in temperature with time for (a) different rotation speeds considering 600 particles and (b) different number of particles considering the rotation speed of 35 rpm.

The numerical simulations were performed only for the case of 800 particles, with rotation speeds of 15 rpm and 55 rpm. The average simulation time was about 140 hours, running with shared memory parallelization (OpenMP) in a cluster with 32 threads. Figure 3 compares the evolution of the temperature rise provided by the numerical solution with the experimental data. The curves of the numerical results consider the average temperature of all particles, and a value of the heat conversion coefficient λ, used in eq. (7), calibrated to reproduce the experimental results with an acceptable agreement. This value was taken as 0.30 for the rotation speed of 15 rpm, and 0.19 for 55 rpm. In both cases, the small value of the conversion coefficient indicates that the ratio of energy dissipated to heat generated is considerably low. However, it must be appreciated that not all forms of heat loss from the particles to the environment are being taken into account in the numerical model, for example, the heat convection with the air is missing. Therefore, if more mechanisms of heat loss were included in the model, the conversion coefficient calibration would give to higher λ values to balance the heat generation with the increase in heat lost. Moreover, this coefficient only quantifies the generated heat that is absorbed by the particles, however in reality, part of the generated heat is directly lost to the environment, for example being absorbed by the air. Nevertheless, the mechanical energy is also dissipated into other types of energy, such as sound.

(a)   (b)
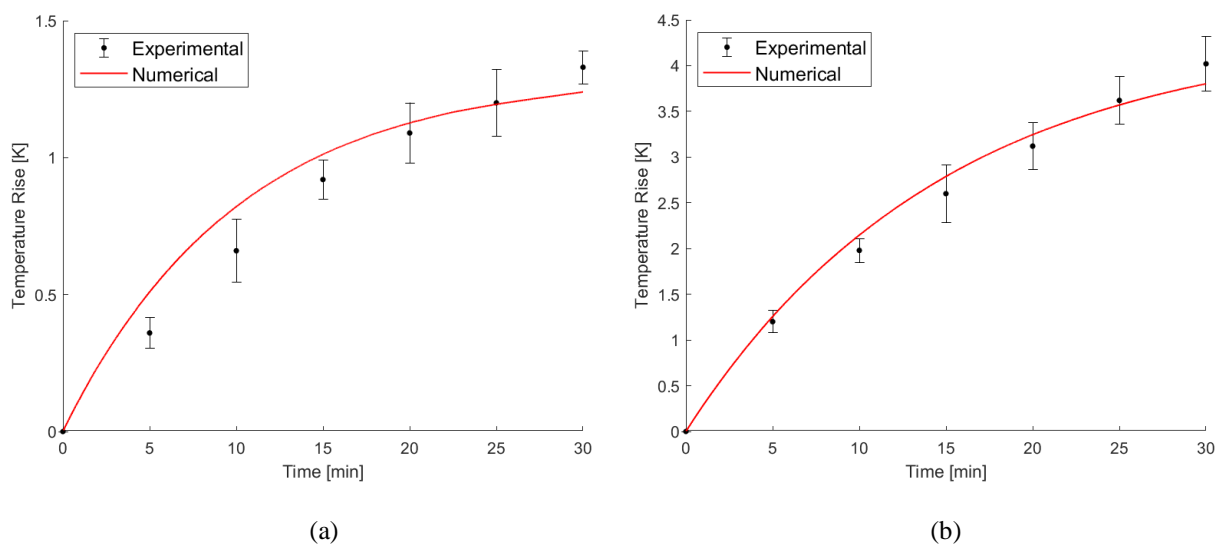
Figure 3. Comparison between numerical results and experimental data: 800 particles with a rotation speed of (a) 15 rpm and (b) 55 rpm.

Figure 4 shows snapshots with the temperature of the particles at the end of the numerical simulations. As seen from the thermal images, the temperature is approximately uniform across all particles at any given time. It validates the assumption made in the experiments that the temperature of a small region of the flow can be taken as representative for all particles. Regarding the mechanical behavior, the computer simulations present the same flow regimes observed in the laboratory tests: rolling regime at 15 rpm, and cataracting regime at 55 rpm.

Figure 5 gives the relative contribution of each heat generation mechanism to the total generation of heat. It is calculated, at each time step, as the ratio of heat generated by a particular mechanism to the sum of all mechanisms. It can be noted that, for both rotation speeds, sliding friction is the mechanism that contributes the most to the increase in the flow temperature, followed by the viscous damping, and rolling friction. It is also interesting to observe that the heat generated from the interactions between particles is always larger than that generated from the interactions between particles and walls, even though the drum is very thin and the particles are constantly in contact with the walls. Furthermore, the flow regime seems to play an important role in the contribution of each mechanism. In the rolling flow, where particles are mostly sliding and rolling against each other, the frictional mechanisms are more relevant. On the other hand, in the cataracting regime, which is dominated by collisions, the contribution of the contact damping forces increases.

(a)   (b)
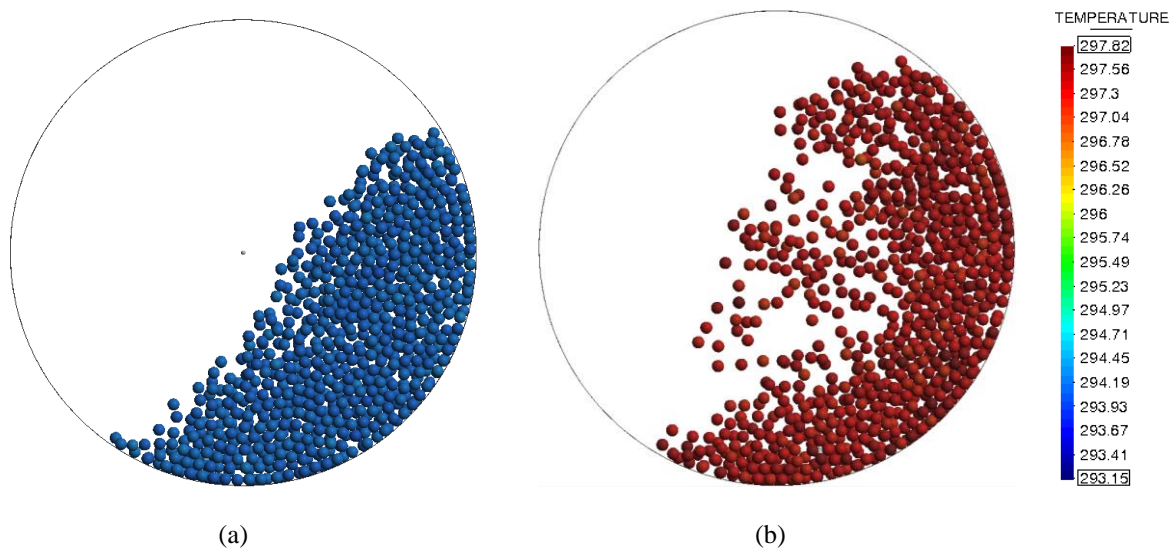
Figure 4. Snapshots from the numerical simulations showing the temperature of the particles after 30 minutes: 800 particles with a rotation speed of (a) 15 rpm and (b) 55 rpm.

(a)   (b)
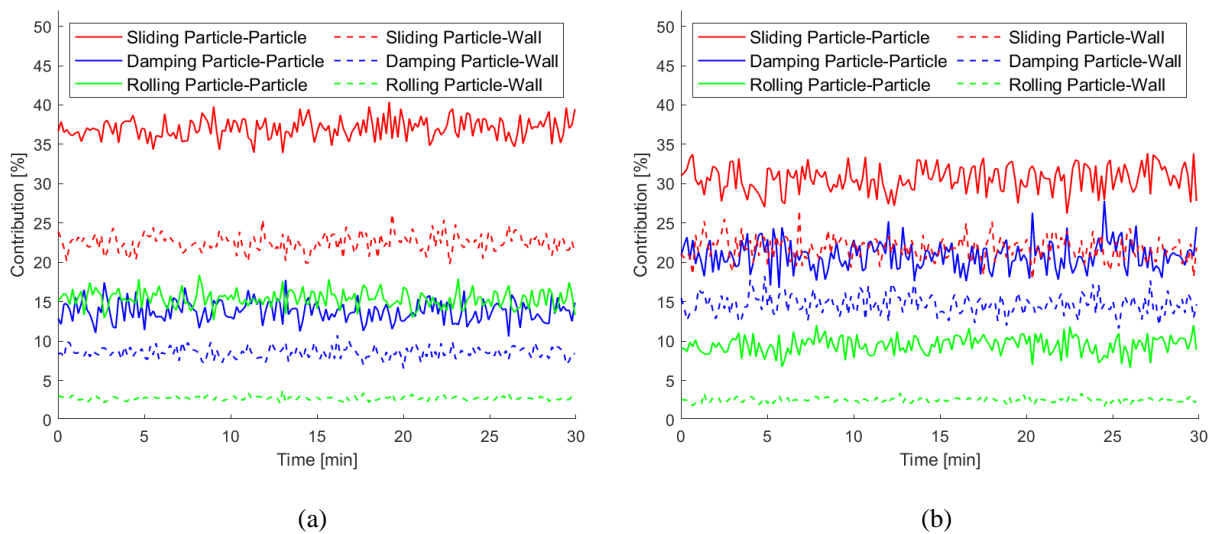
Figure 5. Evolution of the relative contribution of each heat generation mechanism to the total heat generation: 800 particles with a rotation speed of (a) 15 rpm and (b) 55 rpm.

4   Conclusions

This paper has described an experimental and numerical investigation of heat generation by particle mixing in a rotating drum. In the laboratory tests, the effects of rotation speed and filling ratio were explored. It was shown that an increase in the rotation speed, to change the flow regime from rolling to cataracting, leads to a significant increase in the heat generation. The filling ratio, however, has a less significant influence, as an increase in the number of particles results in a slight rise in the flow temperature. The numerical parameters of the simulations were then calibrated, both from the mechanical and thermal point of view, to reproduce the experimental results with different rotation speeds. The conversion ratio of dissipated energy into heat was found to be between 19% and 30%. From the analysis of the relative contribution of each heat generation mechanism, it could be concluded that the particle-particle interactions generate more heat than the particle-wall interactions, with sliding friction being the predominant source, followed by viscous forces and rolling friction. The data may explain the dependency of heat generation on the flow regime, as the fraction of frictional heat tends to increase in the rolling regime, while the contribution from damping forces is more relevant in the cataracting regime.

Some limitations of the numerical modeling presented in this research are the neglect of the heat loss from the particles to the environment by convection with the air, and the assumption that the walls have a fixed temperature throughout the analysis. These limitations can be addressed in future work, together with other modeling improvements, such as the implementation of plasticity as another mechanisms of heat generation. Furthermore, the effects of using different material types for the particles can also be studied.

Authorship statement. The authors hereby confirm that they are the sole liable persons responsible for the authorship of this work, and that all material that has been herein included as part of the present paper is either the property (and authorship) of the authors, or has the permission of the owners to be included here.

References

[1] R. D. Lorenz, "A theory of angel hair: Analytic prediction of frictional heating of particulates in pneumatic transport". *Powder Technology*, vol. 355, pp. 264–267, 2019.

[2] B. Voight and C. Faust, "Frictional heat and strength loss in some rapid landslides: error correction and affirmation of mechanism for the Vaiont landslide". *Geotechnique*, vol. 42, n. 4, pp. 641–643, 1992.

[3] Z. Sun, H. Zhu and J. Hua, "Granular flow characteristics and heat generation mechanisms in an agitating drum with sphere particles: Numerical modeling and experiments". *Powder Technology*, vol. 339, pp. 149–166, 2018.

[4] P. A. Cundall and O. D. Strack, "A discrete numerical model for granular assemblies". G*eotechnique*, vol. 29, n. 1, pp. 47–65, 1979.

[5] ISO 18434-1:2008. Condition monitoring and diagnostics of machines – Thermography – Part 1: General procedures. International Organization for Standardization. URL: https://www.iso.org/standard/41648.html

[6] P. Dadvand, R. Rossi and E. Oñate, "An object-oriented environment for developing finite element codes for multi-disciplinary applications". *Archives of Computational Methods in Engineering*, vol. 17, n. 3, pp. 253–297, 2010.

[7] R. L. Rangel, A. Franci, A. Cornejo, E. Oñate and F. Zárate, "Thermo-mechanical analysis of continuous and discrete media with PFEM and DEM". In: *Proceedings of the joint XLII Ibero-Latin-American Congress on Computational Methods in Engineering (CILAMCE) and III Pan-American Congress on Computational Mechanics (PANACM)*, 2021.

[8] C. Thornton, S. J. Cummins and P. W. Cleary, "An investigation of the comparative behaviour of alternative contact force models during inelastic collisions". *Powder Technology*, vol. 233, pp. 30–46, 2013.

[9] J. Ai, J. F. Chen, J. M. Rotter and J. Y. Ooi, "Assessment of rolling resistance models in discrete element simulations". *Powder Technology*, vol. 206, n. 3, pp. 269–282, 2011.

[10] G. K. Batchelor and R. W. O'Brien, "Thermal or electrical conduction through a granular material". *Proceedings of the Royal Society of London. Series A, Mathematical and Physical Sciences*, vol. 355, n. 1682, pp. 313–333, 1977.

[11] Z. Y. Zhou, A. B. Yu and P. Zulli, "A new computational method for studying heat transfer in fluid bed reactors". *Powder Technology*, vol. 197, n. 1-2, pp. 102–110, 2010.

[12] R. Y. Yang, A. B. Yu, L. McElroy and J. Bao, "Numerical simulation of particle dynamics in different flow regimes in a rotating drum". *Powder Technology*, vol. 188, n. 2, pp. 170–177, 2008.